Nuclear Instruments and Methods in Physics Research A 343 (1994) 135–151
North-Holland

NUCLEAR
INSTRUMENTS
& METHODS
IN PHYSICS
RESEARCH
Section A

Properties of reflective and semitransparent CsI photocathodes

C. Lu *, K.T. McDonald
Joseph Henry Laboratories, Princeton University, Princeton, NJ 08544, USA

Various aspects related to the quantum efficiency of the reflective and semitransparent CsI photocathodes have been investigated experimentally. The investigation explored the dependence of the quantum efficiency on the following: the thickness of the photocathode film, the gas used in the parallel-plate avalanche chamber, exposure to water vapor, and the density of the CsI film. With reflective CsI photocathodes quantum efficiencies of more than 25% at 180 nm have achieved in three different gases: CH_4, C_2H_6, and C_4H_{10}. Our study reveals that high quantum efficiency is also achievable for the semitransparent CsI photocathodes. For a 95-Å semitransparent photocathode the quantum efficiency at 185 nm can be as high as 20%. A simple model to explain the dependence of quantum efficiency on the thickness of CsI photocathodes is suggested, which may be a useful guide for further improvement of the performance of CsI photocathodes Also reported are UV-transmittance measurements for various materials used in our studies, such as methane, ethane, isobutane, CF_4, CO_2, helium, neon, air, TMAE vapor, thin CsI films, and quartz windows, all in the wavelength range 115 nm to 230 nm.

1. Introduction

In the past few years a readout for ring-imaging Cherenkov (RICH) detectors [1] based on CsI photocathodes has been under intensive development [2–17]. The detector is a parallel-plate avalanche chamber (PPAC) with a UV-sensitive solid-CsI photocathode separated by a narrow gap (1–2 mm) from a wire-mesh anode plane (or wire anode plane as in ref. [4]). The Cherenkov light generated in a radiator enters this PPAC through a UV window, passes through the anode mesh, and is detected by the CsI photocathode.

The quantum efficiency of the CsI photocathode is one of the most critical issues for successful operation of this type of detector. Several groups have made impressive progress in this regard. A quantum efficiency as high as 35–40% at $\sim$ 170–180 nm has been reported [4,14] for reflective CsI photocathodes. Recently Charpak et al. reported on investigations of semitransparent CsI photocathodes [11] with somewhat discouraging results: semitransparent CsI photocathodes having much more modest quantum efficiency than reflective ones. Therefore an interesting question has been raised: Why is a CsI photocathode more effective when reflective rather than semitransparent?

Our investigations of CsI photocathodes include the dependence of the quantum efficiency on the following: the thickness of the photocathode film, the gas used in the PPAC detector, exposure to water vapor, and the density of the CsI film. The study of the thickness dependence of the quantum efficiency for semitransparent photocathodes reveals that CsI has a relatively short ($\lesssim$ 100 Å) electron escape length, which is comparable to the optical absorption length. The optimum thickness for a semitransparent CsI photocathode is then of this magnitude also. For 95-Å semitransparent photocathodes the quantum efficiency at 185 nm has been observed to be as high as 20%.

The performance of photodetectors based on CsI is also very sensitive to the UV transparency of the materials in the optical path. To aid in the detector design we have measured the UV transmittance for methane, ethane, isobutane, CF_4, CO_2, helium, neon, air, TMAE vapor, this CsI thin films, and quartz windows, all in the wavelength range 115–230 nm.

2. Investigations of reflective CsI photocathodes

Some of our results in this area have been previously reported [17]. Here we present some extension of that work.

2.1. Experimental set-up

The quantum efficiency of CsI cathodes can be measured by comparison to that of TMAE gas, which has a similar dependence of quantum efficiency on wavelength and whose absolute quantum efficiency has been reported by Holroyd et al. [18]. The apparatus used in our measurement is shown in Fig. 1, and is

* Corresponding author.

SSDI 0168-9002(93)E0819-E

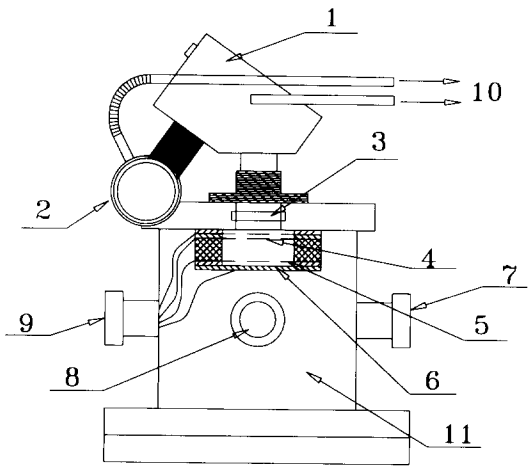

Fig 1. The test chamber for measurement of the quantum efficiency of CsI photocathodes in a parallel-plate avalanche chamber operated with various gases. 1: monochromator; 2: hydrogen lamp; 3: UV window; 4: mesh; 5: anode mesh; 6: photocathode; 7: vacuum port; 8: gas port; 9: signal and HV port; 10: to nitrogen gas bottle; 11: SS vacuum chamber.

based on a design of Hoeneisen et al. [5] of a double-gap chamber that can be used with either a CsI photocathode or TMAE photosensitive gas.

UV light is derived from a pulsed ($\approx$ 400 Hz) hydrogen lamp (Hamamatsu) and the desired wavelength is selected with a monochromator (Instruments SA model H1060). For studies near 170-nm wavelength, the cut-off of UV-grade quartz, all light paths must be in nitrogen. The chamber was pumped down with a Balzers TSH180 oil-free molecular-drag/diagphragm pump system to 5×10^{-5} Torr. The chamber was baked at 60°C every night between data runs, and the photocathode could also be heated to 60°C by a flexible Kapton heating pad (Omegalux KHLV101-10) attached to the back side of the photocathode. Data were taken only after a few days of baking at which time the moisture level inside the chamber was less than 1 ppm, the lower limit of sensitivity of our Kahn Cermet hygrometer. All of the hydrocarbon gases used in this study were scientific grade (MG Industries) with minimum purity of: methane 99.9995%; ethane 99.95%; isobutane 99.96%; and helium 99.999%. The hydrocarbon gas was admitted to the chamber through Oxisorb (MG Industries); according to manufacturer's specification the discharge gas purity should be < 0.1 ppm O_2 and < 0.5 ppm H_2O when used with scientific-grade gases.

For measurement of the relative quantum efficiency of the CsI photocathode, it was held at negative high voltage and the anode mesh was grounded as shown in Fig. 2a. The chamber was filled with a gas mixture and the event rate recorded while varying the wavelength of the monochromator from 170 to 220 nm. The trigger rate of the hydrogen lamp was also recorded. The output of the hydrogen lamp was attenuated by a pin hole and a neutral-density filter until the event rate was less than one out of 10 triggers. Thus we studied the effect of single photons in over 90% of the events.

We next measured the relative quantum efficiency of TMAE gas. For this the CsI-coated electrode was used as an anode and was set at positive high voltage as shown in Fig. 2b. The wire mesh that previously served as the anode remained grounded, but now functioned as a grid. The other wire mesh, which previously played no role, was now set at -250 V. The 2.03-cm-thick region between this mesh and the grounded mesh served as the photodetection and transfer area. TMAE vapor was admitted into the evacuated chamber until the vapor pressure reached $\approx$ 400 mTorr. The actual TMAE vapor pressure was measured by an Edwards model 600A capacitance manometer. Then the chamber was filled with hydrocarbon gas to the desired pressure. UV photons were absorbed by TMAE vapor, converted to photoelectrons, and drifted towards the

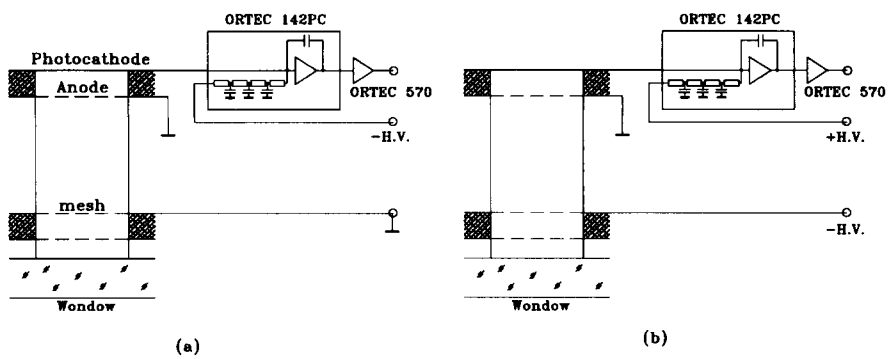

Fig. 2. The high voltage arrangement for quantum-efficiency measurement: (a) CsI photocathode mode; (b) TMAE mode.

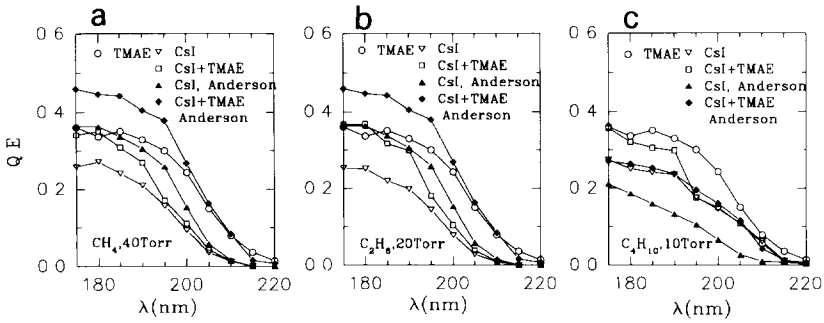

Fig. 3. The quantum efficiency of CsI (a) in CH_4, (b) in C_2H_6, and (c) in C_4H_{10}. Also shown are data points from Anderson et al. [14].

grounded mesh without significant multiplication in the weak electric field. After passing through the grounded mesh they entered the avalanche region and were subsequently detected at the anode.

The photon absorption spectrum of TMAE is rather flat from 170 to 220 nm [18], and we took the average value of the absorption coefficient μ to be 0.488 /cm for 400-m Torr TMAE. From the geometry of our test chamber and transparency of the meshes we calculated the portion of UV light absorbed by the TMAE vapor in the transfer region. Using the known quantum efficiency of TMAE [18] and the ratio of the event rates of CsI mode and TMAE mode in the test chamber, the quantum efficiency of CsI photocathode was derived.

In a third set of measurements the quantum efficiency of CsI photocathodes with an absorbed layer of TMAE was determined. For this we started with the TMAE-mode measurements, and then restored the electrodes to the CsI-mode configuration without changing the chamber gas. Photoelectrons produced in the transfer region did not produce avalanches in this configuration. A correction was made for the substantial attenuation of the UV light in the transfer region, thereby deriving the quantum efficiency for CsI + TMAE cathodes also reported in Fig. 3.

2.2. Effect of different gases on the quantum efficiency

We have used the apparatus described above to measure the quantum efficiency for three different gases: methane, ethane and isobutane. The results are summarized in Fig. 3.

We do not find as big a difference between the quantum efficiency in CH_4 and C_4H_{10} as reported by Anderson et al. [14]; the quantum efficiency of our photocathode in CH_4 is lower than theirs, while in C_4H_{10} it is higher than theirs. The thickness of our photocathode was 5000 Å.

2.3. Effect of water vapor on the quantum efficiency

Because of the large band gap of CsI (≈ 6 V), it is believed that CsI photocathodes do not oxidize on exposure to air. The observed reduction of the quantum efficiency on exposure to air is mainly blamed on the effect of water vapor.

We studied this effect by exposing the chamber to a controlled amount of water vapor for 15 minutes. Then we pumped down the chamber, filled it with the working gas, and measured the quantum efficiency. Next, the whole chamber was heated up to 60°C with an infrared lamp; the photocathode could also be heated by a heating pad mounted on the back of the photocathode plate. After various intervals the chamber was reactivated with gas and the quantum-efficiency measurement repeated. The recovery of the quantum efficiency vs. time of heating is shown in Fig. 4.

The saturated water vapor pressure at room temperature is ~ 24 Torr, so the three vapor pressures used in our investigation represent three humidity conditions: very dry, modest, and very humid. For the 2-Torr case the recovery was very quick; within an hour

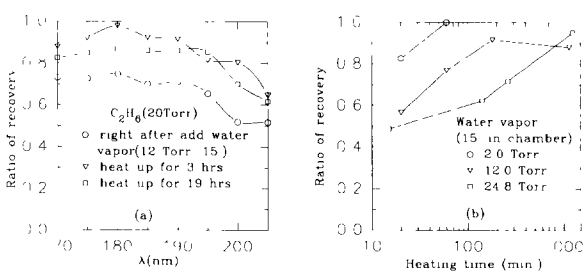

Fig. 4. The effect of water vapor on the quantum efficiency of CsI. (a) The recovery ratio vs. wavelength for a photocathode exposed to 12 Torr of water vapor for 15 minutes. (b) The recovery ratio vs. heating time after exposures to various amounts of water vapor for 15 minutes.

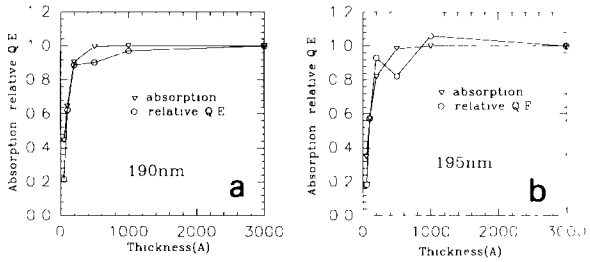

Fig. 5. The UV absorption and quantum efficiency of CsI films vs. film thickness (a) at 190 nm, and (b) at 195 nm.

the quantum efficiency was completely restored. Even for the case of 100% humidity, after 19 hours of heating at 60°C more than 90% of the quantum efficiency was recovered. However, extremely humid conditions should be avoided, otherwise the CsI photocathode can be damaged permanently, as discussed in section 4.4.

2.4. Effect of photocathode thickness on quantum efficiency

Six different thicknesses of CsI photocathodes have been tested: 50, 100, 200, 500, 1000 and 3000 Å. We also measured the transmittance for those six thicknesses of CsI films when evaporated onto a UV quartz window. The spectrophotometer used in this study is Perkin-Elmer model λ3. This is not a vacuum UV spectrometer; therefore the shortest wavelength is limited at 190 nm. We plot the percentage absorption of UV light and the relative quantum efficiency at 190 and 195 nm wavelengths vs. thickness of the CsI film in Fig. 5. It is clearly seen that the thickness of the film need not be very large. By 200 Å the film has already reached more than 80% of the maximum quantum efficiency. The quantum-efficiency curve follows the absorption curve rather closely, but the quantum efficiency increases more quickly with the thickness than

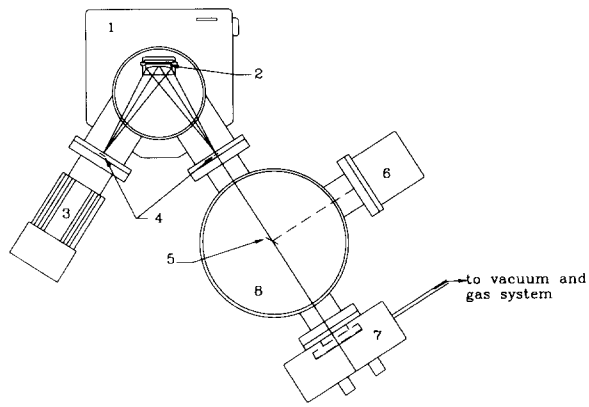

Fig. 7. Sketch of the VUV monochromator. 1: Model 234/302 0.2 m vacuum monochromator; 2: Halographic grating; 3: model 632 deuterium source unit; 4: entrance and exit slits; 5: UV mirror; 6: model 654 side-on PMT detector with sodium salicylate screen; 7: test chamber (semitransparent or reflective photocathode); 8: vacuum compatible sample chamber.

does the absorption curve for the first 200 Å. An explanation for this is presented in section 4.5 below.

2.5. Effect of the density of CsI film on the quantum efficiency

During studies in the early 1960s low-density KCl films showed enhanced secondary emission [19,21]. Interpretations were given that the internal electric field in a "fluffy" film might enhance the secondary emission, and/or that the transport of the secondary electrons is more favorable than in normal-density films.

We have studied several "fluffy" films in our laboratory. For full-density CsI films the secondary emission ratio was observed to be ~20 (as reported by many others). With a low-density CsI film (5% of normal density) the secondary emission ratio was observed to be as high as 100. Details of this work are beyond the scope of this paper.

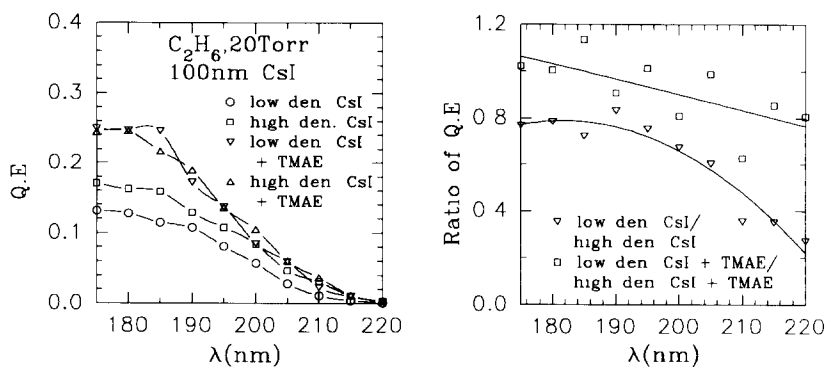

Fig. 6. The measured quantum efficiencies of high- and low-density CsI photocathodes.

An immediate question is whether "fluffy" CsI films would show enhanced photoemission. To answer this we made a low-density CsI film of 1000-Å effective thickness (i.e., the same area density as a normal film of that thickness). Instead of performing the CsI evaporation under good vacuum, we filled the bell jar with ~ 10 mTorr Ar. The "fluffy" film was deposited in two minutes at a rate of ~ 4 to 10 Å/s. The CsI film was examined under a microscope, and the thickness was estimated to be 20 times that of a 0.1-μm full-density film; i.e., the density was ≈ 5% of normal.

The measured quantum efficiencies of 1000-Å high- and low-density CsI photocathodes are summarized in Fig. 6. The quantum efficiency of the low-density CsI film was only ~ 80% of high-density one. Certainly more carefully studies need to be done before drawing definitive conclusions about low-density photocathodes.

3. UV-absorption measurements for various materials

After the work described above was completed we obtained a vacuum UV monochromator. This device has proved to be extremely useful in clarifying the behavior of CsI photocathodes at short wavelengths.

A sketch of the McPherson model 234/302 vacuum monochromator is shown in Fig. 7. The deuterium light source has a MgF_2 window. The whole system can be pumped down to less than 1 mTorr by a molecular-drag pump to eliminate the absorption of UV light by oxygen. When measuring the absorption spectra for different materials, the photomultiplier (PMT) detector was placed at the front port of the sample chamber, and the side port was sealed. The UV mirror indicated in the figure was replaced by the sample, such as a CsI-coated LiF window, a quartz window, or a vacuum-compatible 10-cm-path-length gas sampling cell

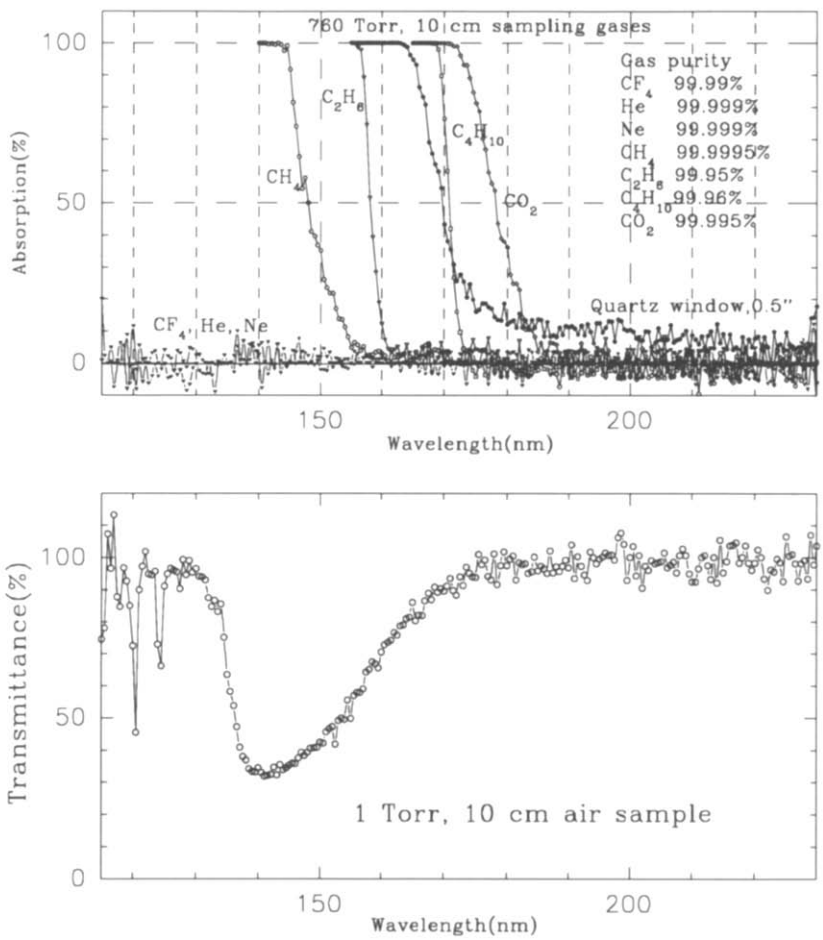

Fig. 8. The UV absorption spectra for various materials.

with MgF_2 windows, etc. The gas sampling cell could be to pumped down to $\sim 10^{-5}$ Torr by a turbo/molecular-drag pump. A sodium salicylate wave-shifting screen was mounted in front of a Hamamatsu model 1P28 side-on phototube, permitting the PMT detector to sense photons of wavelengths down to 115 nm. The long-term stability of the phototube and the deuterium lamp was checked every day routinely, and was quite satisfactory.

The measured UV absorption spectra are summarized in Fig. 8. Note that isobutane has higher absorption than quartz between 165 nm and 172 nm. Also shown is the transmittance of a 1-Torr, 10-cm air sample, for which a large transmittance dip between 130 nm and 180 nm is clearly seen.

3.1. Transmittance of CsI films

We measured the transmittance of 51-, 100- and 310-Å-thick CsI coatings evaporated onto thin LiF windows, with results summarized in Fig. 9a. The absorption lengths of CsI coatings deduced from those transmittance curves are shown in Fig. 9b and are reasonably consistent. For CsI photocathodes used with quartz windows the wavelength region of interest is 165 to 220 nm, over which the absorption length varies between 100 and 200 Å.

We also compared the transmittance of a freshly made CsI film and that of the same one after exposure to air for 14 hours. As seen in Fig. 10 the transmittance was reduced by $\sim 10\%$ after 14 hours.

3.2. The extinction coefficient of TMAE vapor

The TMAE sample was obtained from the RSA Corporation. The original liquid had a much higher saturated vapor pressure than TMAE, indicating the presence of impurities that have higher vapor pressure. According to advice from D. Anderson, we washed the sample with distilled water under a N_2 atmosphere.

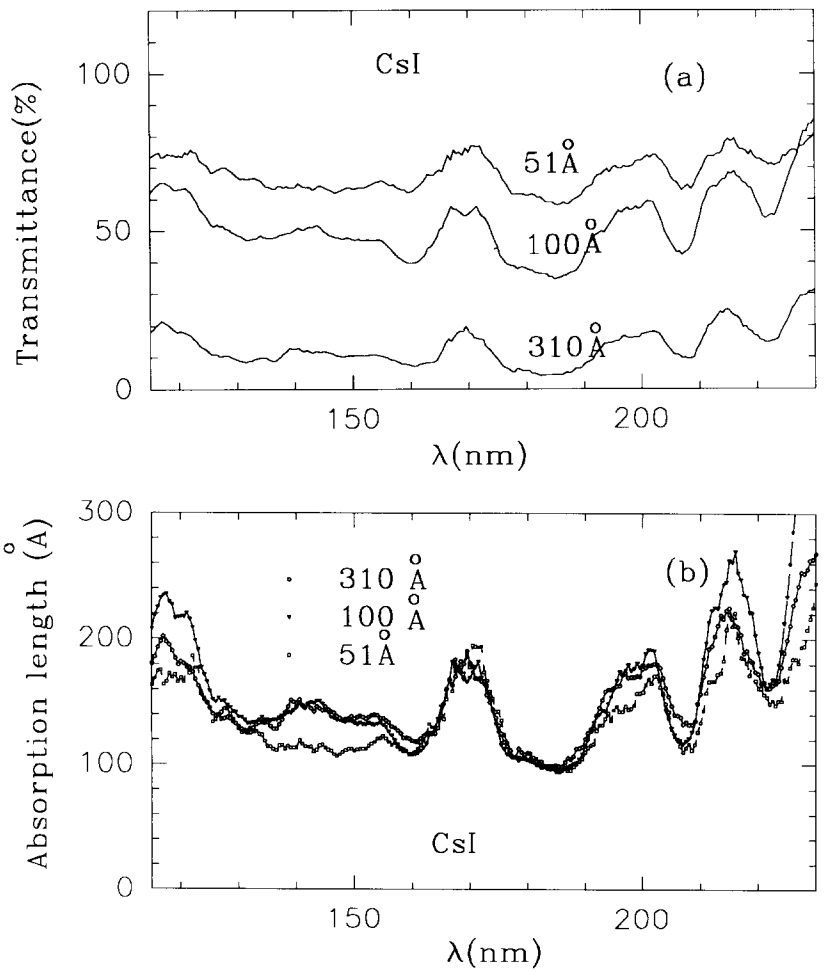

Fig. 9. The transmittance curves of three CsI coatings: (a) transmittance; (b) absorption length.

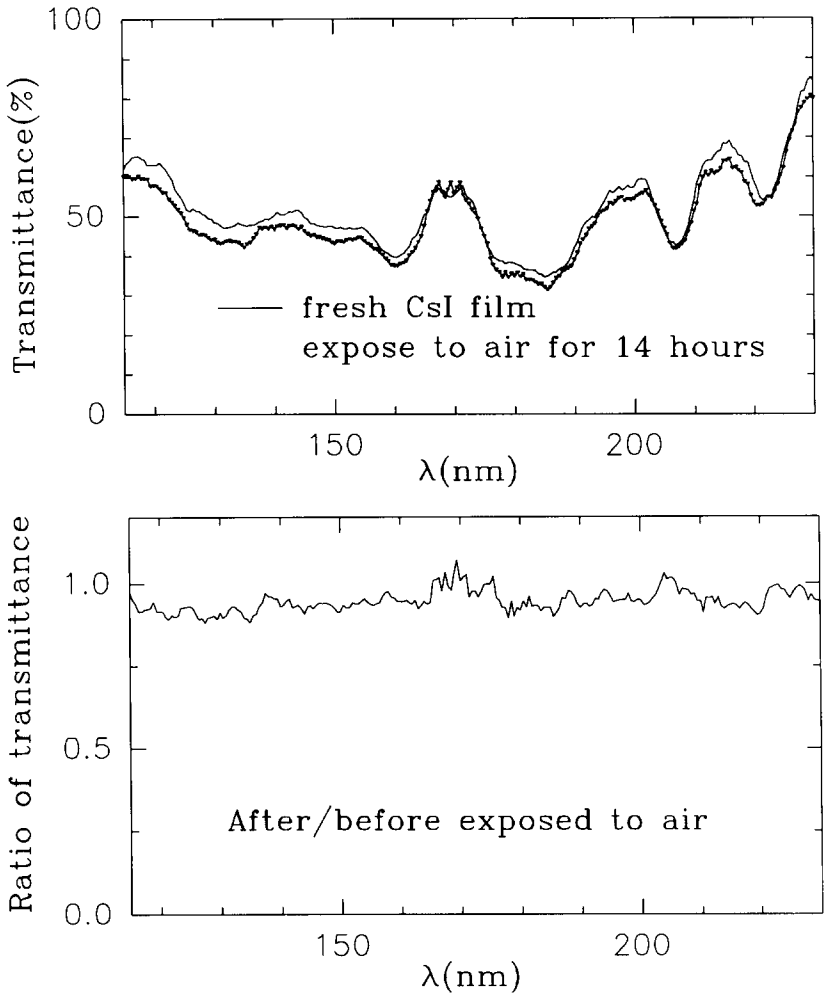

Fig. 10. The transmittance of a 100-Å-thick CsI coating after exposure to air for 14 hour.

The lower wash layer of water was clearly separated from the upper layer of TMAE. The color of the wash layer was quite clear, so we only washed once. We then bubbled N_2 gas through the sample while pumping out the N_2 gas through a cold trap. After 15 hours of such treatment, the liquid level was reduced by ~ 20%. We found the resulting sample to have a saturated vapor pressure very close to that of TMAE [22].

To measure its transmittance, TMAE vapor was admitted to the sampling cell of the VUV monochromator after it was first pumped down to less than 10^{-5} Torr. After the spectrum scan, the sampling cell was pumped down overnight, and then the transmittance was measured for the empty cell. Because of the adsorption of TMAE on the surface of the MgF_2 windows, the second spectrum was quite different from the one taken before admitting TMAE vapor. We used the last spectrum as the reference when calculating the TMAE absorbance, which is defined as $A = \log_{10}(1/T)$, where T is the transmittance.

To compare our results with previous work, we also calculated the extinction coefficient ϵ, which is related to the absorbance by $A = \epsilon cl$, where c is the gas concentration in moles per liter and l is the length of the gas sample. The results are shown in Fig. 11, along with results from other authors [18,23]. Similar results to Holroyd et al. were published by Arnold et al. [24], which are not shown in our figure. The general shape of our curve is similar to the others, but our values are generally lower. A large discrepancy between our data

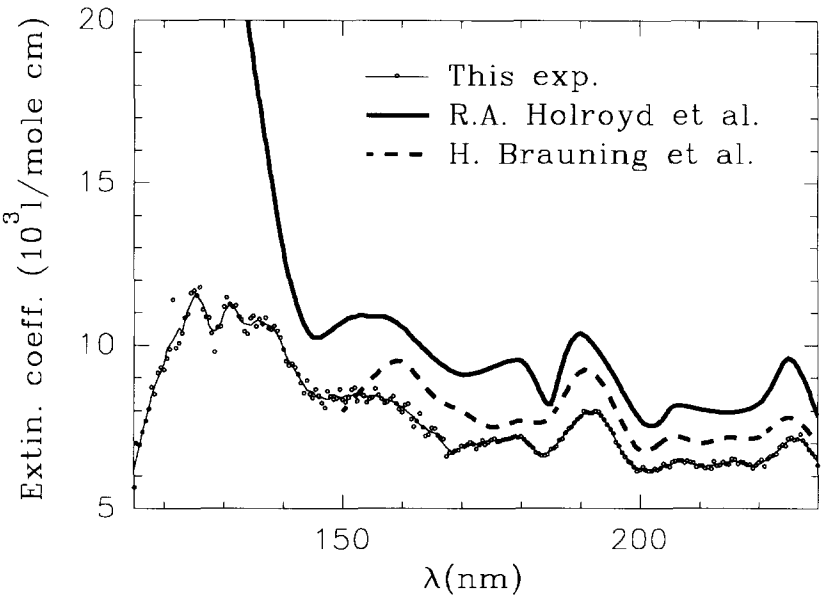

Fig. 11. The extinction coefficient ϵ of the TMAE. The absorption cross section $\sigma(\text{mb}) = 3.82\ \epsilon\ (\text{m}^3/\text{mole-cm})$.

and that of Holroyd et al. is seen below 140 nm where their curve increases sharply. No data are available below 150 nm from Bräuning et al. and Arnold et al.

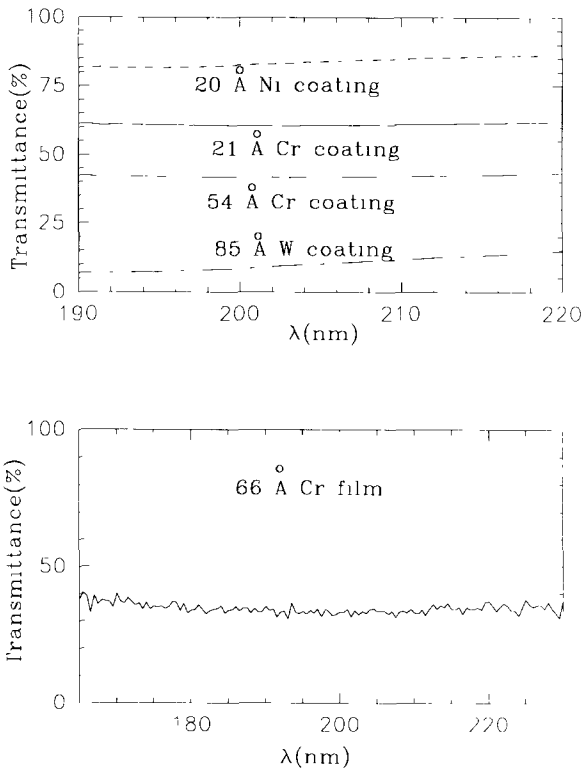

Fig. 12. The transmittance of three thin metal films.

3.3. The transmittance of thin metal films

To prepare semitransparent CsI photocathodes we need a good UV-transparent conductive thin metal film as a substrate. We investigated three metals, tungsten, nickel and chromium, which are presently used for this purpose in industry. Thin films were evaporated onto quartz windows either with an electron gun (tungsten), or with a heated boat (nickel and chromium). Transmittance measurements are shown in Fig. 12a taken with a Perkin-Elmer model λ3 spectrophotometer, which is limited to wavelengths longer than 190 nm.

For our studies of semitransparent photocathodes we used a 66-Å-thick Cr film, and measured its transmittance with a VUV monochromator with results as shown in Fig. 12b. The lower bound of the spectrum was set at 165 nm by the transmittance of quartz windows.

The resistivities of those films were measured with an Alessi C4S four-point probe [25]. Only the Cr films show promising results: $\rho_s = 0.3$ MΩ/□ for 21-Å Cr, $\rho_s = 0.08$ MΩ/□ for 54-Å Cr. For two other films the resistivities were too large to determine with this set-up.

4. Investigations of semitransparent CsI photocathodes

4.1. Experimental set-up

The experimental set-up employed in this investigation is sketched in Fig. 7 and details of the chamber

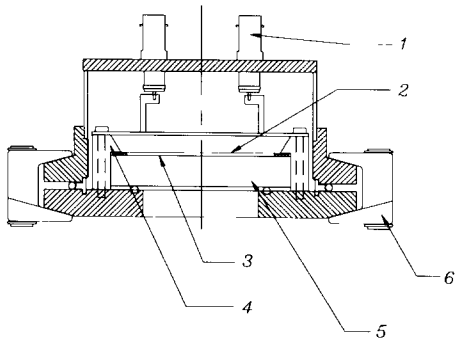

Fig. 13. The semitransparent-photocathode test chamber. 1: SHV connectors; 2: mesh as anode; 3: Cr coated surface; 3: Teflon clamp; 5: quartz window of 3 in. diameter and 0.5 in. thick; 6: chain clamp.

are shown in Fig. 13. One surface of a half-inch-thick quartz window was coated with a 66-Å-thick Cr film. Around the periphery of the surface a 0.25-in.-wide Al ring (1000 Å thick) was evaporated on the top of the Cr film. The rest of the surface area was evaporated with CsI.

The cathode was separated from the anode by a 1.6-mm-thick copper-clad G-10 ring, to the other side of which was soldered an 80% transparent stainless-steel mesh. By tightly compressing this ring together with the coated side of the window, a PPAC with CsI coating as photocathode and the mesh as anode was formed. A similar chamber with two meshes and a reflective photocathode was also constructed, with an electrode arrangement as shown in Figs. 1 and 2. As a reference for the measurement of the quantum efficiency of the semitransparent photocathode in the first chamber, the second chamber was filled with TMAE vapor, following the procedures discussed in section 2 above.

The UV mirror at the center of the sampling chamber (Fig. 7) could be inserted to deflect the light to the side port, or removed to permit light to exit the front port. A PMT detector at the side port could thereby monitor the light intensity from day to day, which proved to be quite stable so that no correction was necessary.

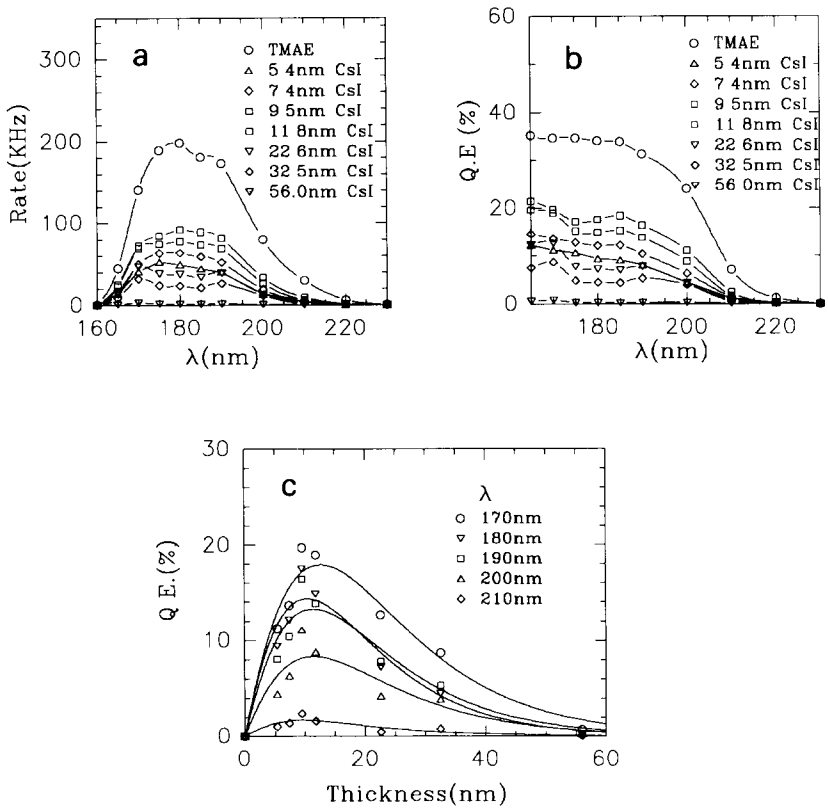

Fig. 14. The quantum efficiency of semitransparent CsI photocathodes: (a) event rate vs. wavelength for TMAE vapor and seven CsI films; (b) quantum efficiency vs. wavelength for TMAE vapor (from ref. [18]) and seven CsI films; (c) quantum efficiency vs. CsI thickness at five wavelengths.

4.2. Effect of thickness of the semitransparent CsI film on quantum efficiency

The signal from the test chamber with a semitransparent CsI photocathode was analyzed by an EG&G ORTEC multichannel analyzer system, which included a model 142PC charge-sensitive preamplifier, a model 570 spectroscopy amplifier, and a model 916 multichannel analyzer. The entrance slit of the monochromator was set at 5 μm, and the exit slit was 0.03 mm. A neutral-density filter of optical density ~ 1 was placed in front of the UV mirror to further reduce the light intensity so that individual photoelectron-induced avalanches could be detected.

At each wavelength a spectrum was recorded of the charge produced in the chamber per photoelectron. These spectra had clear peaks and were well described by Polya distributions [17]. The observed rate of photoelectrons as a function of wavelength is plotted in Fig. 14a for eight CsI coatings with thicknesses 54, 74, 95, 118, 226, 325, and 560 Å. No signal could be discerned from a film of 2000 Å thickness.

Data were also taken with the double-mesh chamber filled with TMAE vapor, whose known quantum efficiency provided a normalization for the measurements with the semitransparent CsI films. A correction has been made for the light absorbed in the Cr film, so the results displayed in Figs. 14b and 14c are for the quantum efficiency of the CsI film only.

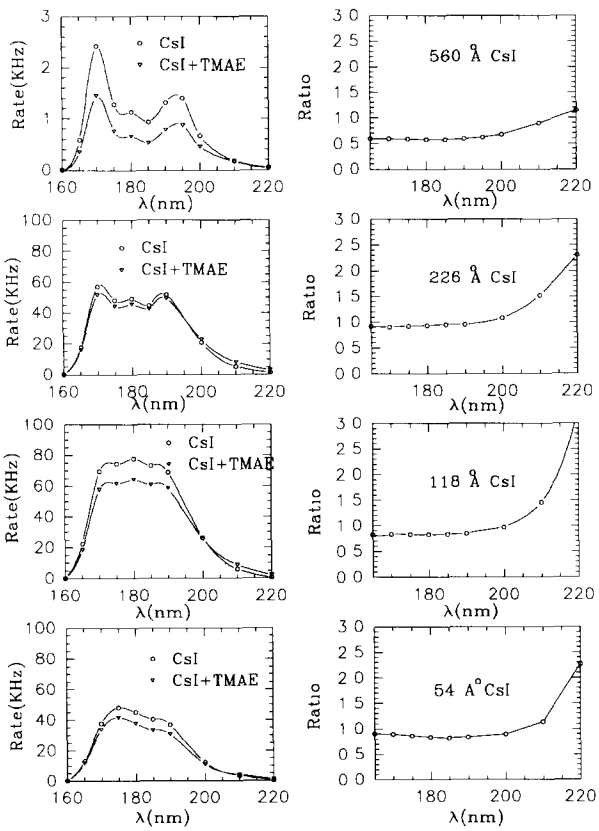

Fig. 15. The effect of adsorbed TMAE on the quantum efficiency of semitransparent CsI photocathodes.

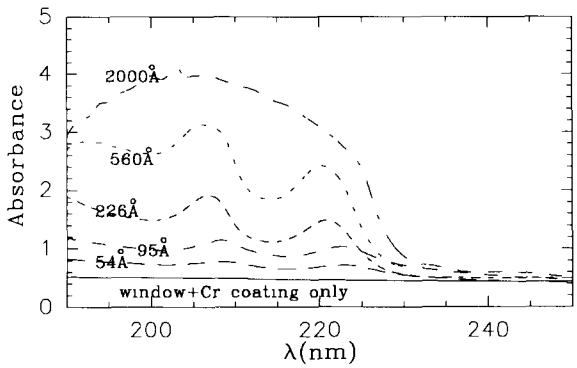

Fig. 16. The absorbance of semitransparent CsI films.

The quantum efficiency of a 95-Å-thick semitransparent CsI photocathode was observed to be about 20% for 165–185 nm, except a small dip around 175 nm. The gas used in this chamber was C_2H_6. Our previous studies on reflective CsI photocathodes showed that the highest quantum efficiency observed with ethane gas was ~ 26% at 175 nm (see Fig. 3). For semitransparent CsI photocathodes thicker than 100 Å the quantum efficiency falls off rapidly with thickness. While a 2000-Å thickness is often used for reflective CsI photocathode studies, a semitransparent CsI photocathode of this thickness shows essentially zero quantum efficiency.

4.3. Quantum efficiency for semitransparent CsI films with adsorbed TMAE

An adsorbed layer of TMAE on reflective CsI photocathodes can increase the quantum efficiency by

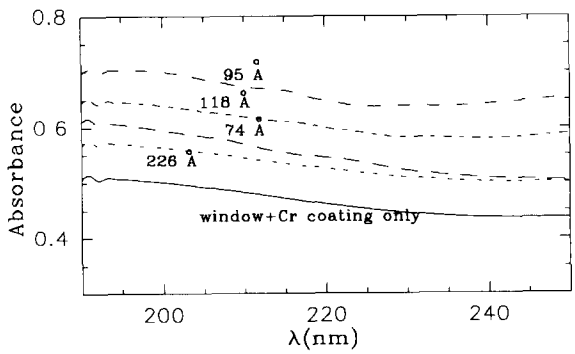

Fig. 17. The absorbance of highly moisturized CsI films. They are largely transparent to UV light.

~ 25% [4,14]. The actual mechanism for this effect is still not completely clear.

We studied this effect with four semitransparent CsI photocathodes. After pumping down the chamber to vacuum, TMAE vapor was admitted and then the chamber was filled with 20 Torr C_2H_6. The observed rates of photoelectrons vs. wavelength are shown in Fig. 15 for four cathode thicknesses. It appears that the quantum efficiency in the range 165–200 nm is lower than that for clean CsI photocathodes, but for 200–220 nm the quantum efficiency for CsI + TMAE is higher than for clean CsI films.

4.4. Transmittance of moisturized CsI films

When, we finished the quantum-efficiency measurement for each semitransparent CsI photocathode, the absorbance of the CsI-coated window was measured immediately with a Perkin-Elmer λ3 spectrophotometer. The absorbance curves are shown in Fig. 16. If the CsI film was exposed to an extremely humid atmosphere (such as the human breath), the appearance of the film turned milky immediately, and the UV absorbance of the film was destroyed completely (i.e., it became transparent to UV light). Measurements of the absorbance of several highly moisturized CsI films are shown in Fig. 17. According to our preliminary observation, once the films became UV transparent due to moisture, their former absorbance could not be restored by heating. This is in contrast to the results of section 2.3 for films exposed to $\leq 100\%$ humidity.

4.5. Discussion

A more clear picture of the CsI photoemission mechanism has emerged with the data obtained from the semitransparent photocathode studies. The UV absorption length of CsI films is 100–200 Å. The photoelectrons released by the UV photons suffer many collisions, elastic and inelastic, before being captured inside the film or finally approaching the surface and escaping.

To describe the latter process we use a parameter L, the escape length. The escape probability for a photoelectron produced at distance x from the surface of a thick photocathode can be expressed as

$$G(x) = Te^{-x/L},$$

where $T \leq 1$ is the probability that an electron that reaches the surface from inside will escape.

A Monte Carlo calculation of the energy dependence of parameters L and T has recently been performed by Akkerman et al. [15]. In our case, the electron energy relative to the vacuum level (= photon energy − work function of the photocathode) varies from 0 to 2 eV. For such small energies the electron escape length L is calculated to be only ~ 20–200 Å, which is shorter than or similar to the UV absorption length.

We label the intrinsic quantum efficiency of CsI as Q, and the UV absorption length as λ. Then the probability that a photoelectron is produced in a CsI layer dx thick is

$$\frac{Q\,dx}{\lambda}e^{-x/\lambda} \qquad \text{(reflective)},$$

where x is measured from the surface through which the photon entered. For a semitransparent photocathode of thickness d the photon enters through the other surface than the one across which the electron must escape. If we measure x from the surface across which the electron escapes, then the probability that a photoelectron is produced at x is

$$\frac{Q\,dx}{\lambda}e^{-(d-x)/\lambda} \qquad \text{(semitransparent)}.$$

Convoluting this with the escape probability $G(x)$ we arrive at a model of the observed quantum efficiency of a semitransparent photocathode of thickness d:

$$\mathrm{QE}_{\mathrm{obs}} = \frac{QT}{\lambda}\int_0^d e^{-(d-x)/\lambda}\, e^{-x/L}\, dx$$

$$= QT\frac{L}{L-\lambda}(e^{-d/L} - e^{-d/\lambda})$$

(semitransparent).

Using this formula reasonable fits were obtained to the data shown in Fig. 14. The absorption length and the escape length turned out to be similar, ~ 100 Å, and the quantity QT decreased from 44% to 19% as the wavelength increased from 170 to 200 nm.

This simple model does not take the interface between the CsI film and the thin metal substrate into account. In reality an electron that reaches the metal substrate is likely captured there, while in the model it has an implied nonzero probability to penetrate into the metal and scatter back into the CsI. Hence one should not consider the numerical values for L and λ deduced above as overly precise. But since the model does fit the experimental data quite well, we believe the overall picture of this model is correct.

A more sophisticated model based on the diffusion equation can be used to describe the photoelectron transport process in the CsI film (see the Appendix). In this model the expression for the observed quantum efficiency of a semitransparent photocathode becomes

$$\mathrm{QE}_{\mathrm{obs}} = \frac{QTL}{2\sinh d/L}$$

$$\times\left(\frac{1-e^{d/L-d/\lambda}}{L-\lambda} - \frac{1-e^{-d/L-d/\lambda}}{L+\lambda}\right)$$

(semitransparent).

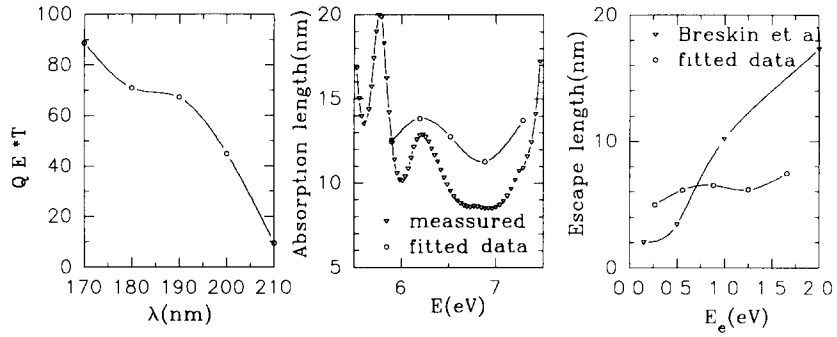

Fig. 18. Results of fitting the observed quantum efficiency of semitransparent CsI photocathodes to a diffusion model. The UV photon energy is labelled as E. The photoelectron energy E_e is measured with respect to the vacuum level, so $E_e = E - \phi$ where the work function $\phi \approx 5.6$ V corresponds to about 220 nm. The "measured" optical absorption length for CsI is taken from Fig 9.

The parameters fitted to the data of Fig. 14 with the diffusion model are summarized in Fig. 18 along with the escape length taken from a Monte Carlo calculation by Akkerman et al. [15]. In this model an electron that reaches the interface between the CsI and metal films will be captured by the metal film immediately.

According to the diffusion-model fits the values of QT are very high. Recall that Q is the intrinsic quantum efficiency that a photon absorbed in CsI produces an electron that moves away from the photoabsorption site. Because of the short escape length in CsI the observed quantum efficiency is considerably lower than the intrinsic quantum efficiency. Of course, QT cannot exceed unity.

Many groups have measured the quantum efficiency of CsI to be close to that of TMAE vapor. But for TMAE vapor there is no electron escape problem; once a photoelectron leaves a TMAE molecule it has a high probability of being observed. Hence we infer that the intrinsic quantum efficiency of CsI is actually much higher than that of TMAE vapor.

We also can calculate the quantum efficiency of reflective CsI films, and the simple model predicts

$$\mathrm{QE_{obs}} = QT\frac{L}{L+\lambda}(1 - \mathrm{e}^{-d(L+\lambda)/L\lambda}) \qquad \text{(reflective)},$$

for a cathode of thickness d. Because $(L+\lambda)/L\lambda$ is always greater than $1/\lambda$ the quantum efficiency of a reflective cathode increases more quickly with thickness than does the number of absorbed photons. This effect is seen in Fig. 5.

Both models give the same result for thick films:

$$\mathrm{QE_{obs}} = QT\frac{L}{L+\lambda} \qquad \text{(thick, reflective)},$$

which holds so long as the thickness satisfies $d \gg L + \lambda$. If the escape length L is smaller than the optical absorption length λ, the observed quantum efficiency will be markedly less than the intrinsic quantum efficiency. From the results of the fits shown in Fig. 18 it appears that $L < \lambda$ for essentially all wavelengths measured, so $\mathrm{QE_{obs}} \leq QT/2$.

A possible way to increase the observed quantum efficiency of a reflective CsI photocathode is to deposit the CsI on a wedge-like substrate surface, as sketched in Fig. 19. For such a photocathode the photoelectron escape length (measured perpendicular to the local surface) is not changed, but the UV absorption length is effectively decreased by a factor

$$F = \sqrt{1 - \frac{\cos^2\theta}{n^2}},$$

where θ is the wedge angle shown in Fig. 19, and n is the refractive index of CsI. We estimate that $n = 1.6$

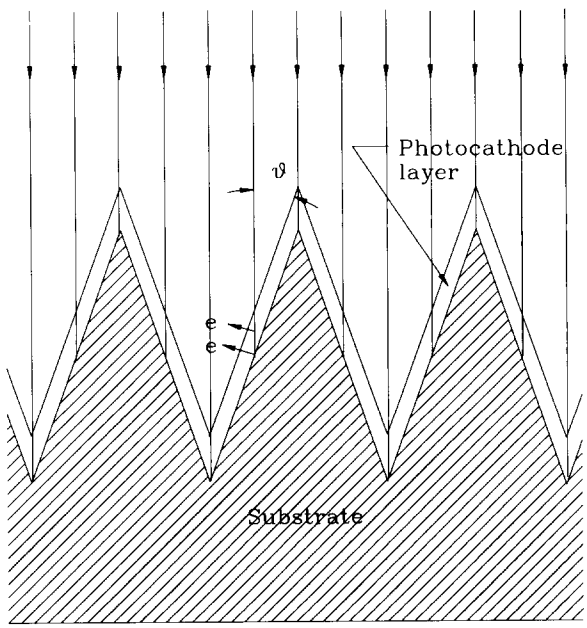

Fig. 19. A wedge-shaped photocathode surface would increase the observed quantum efficiency.

for CsI, so that if $\theta = 20°$, then $F = 0.81$. For wavelengths such that $\lambda = 2L$ the quantum efficiency observed with a flat surface is only 0.33 of the intrinsic quantum efficiency, but with the wedge-shaped photocathode it would rise to 0.38, a 15% improvement.

When a CsI photocathode is used to detect Cherenkov light from a liquid or solid radiator, the light will have non-normal incidence. This automatically improves the quantum efficiency compared to that inferred from studies with normally incident light. Hence we have one more indication of how well suited CsI photocathodes are for use in RICH detectors.

Appendix: models of electron transport in CsI films

We review several models of electron transport in CsI photocathodes.

For very thick films it nearly suffices to characterize the transport by a single "escape length" that we will call L in this note. For thin films more care is needed. An interesting issue is whether electrons that are produced heading away from the surface scatter enough to eventually reverse direction and escape. Also, when semitransparent photocathodes are used the performance is very sensitive to electron transport.

We label *reflective* photocathodes as those for which the signal electrons are collected from the same surface across which the photons enter, and *semitransparent* cathode films as those for which photons enter one surface and electrons are collected from the other.

Accurate modelling of electron transport is based on the Boltzmann transport equation, along with characterization of the various scattering cross sections. However, no analytic solutions are available in this approach, which must be pursued by Monte Carlo calculations. Here we review three one-dimensional models of increasing sophistication: 1) a simple exponential model; 2) a simple diffusion model; and 3) a more intricate diffusion model.

The third model may have sufficient accuracy for the present state of studies of CsI photocathodes for RICH detectors.

A.1. An exponential model

In this model we suppose that an electron which is photoejected at a distance x from the surface has an escape probability of

$$G(x) = T e^{-x/L}. \tag{A.1}$$

We label this probability as G as it is a kind of Green's function for the electron transport. In this, T is the probability that if the electron reaches the surfaces it actually escapes. As CsI has a low electron affinity (≈ 0.1 eV) it is expected that $T \approx 1$. Parameter L is the escape length, which is finite because electrons might be trapped on defects, or more likely just lose energy until they can no longer escape.

Some people consider that the surface-transmission coefficient T is not distinct in origin from the escape length L, and therefore set $T = 1$. We will see below that the factor T cannot readily be isolated from the intrinsic quantum efficiency Q of the photocathode.

Both T and L are in principle functions of the initial energy of the electron, i.e., of the photon energy.

If the photons incident on CsI have an energy more than 12 eV, which is more than twice the band-gap energy, then the photoelectrons can cause secondary emission. In this case the quantum efficiency could appear to be greater than one. In the present note we restrict ourselves to photon energies of only 6–12 eV, and ignore secondary emission.

In Eq. (A.1) we have supposed that electrons can reach the surface no matter what their initial direction. This is plausible if the electron transport is dominated by a large number of electron–phonon interactions that are nearly elastic. This is believed to be the case in an insulator such as CsI, in contrast to a metal where electron–electron scattering is more prominent. The major shortcoming of the exponential model is its oversimplified treatment of the multiple scattering.

The model is completed by noting that the probability that an electron is created in an interval dx at depth x from the surface by a normally incident photon is

$$Q \frac{dx}{\lambda} e^{-x/\lambda}, \tag{A.2}$$

where λ is the optical absorption length, and Q is the intrinsic quantum efficiency. Both λ and Q are functions of the energy of the photon.

Hence the expected yield Y_R of electrons per photon in a reflective photocathode of thickness d is

$$\begin{aligned} Y_R &= \frac{Q}{\lambda} \int_0^d dx\, G(x)\, e^{-x/\lambda} \\ &= QT \frac{L}{L+\lambda} (1 - e^{-d/L - d/\lambda}). \end{aligned} \tag{A.3}$$

The maximum yield in reflection mode is then achieved with a very thick photocathode, and has the value

$$Y_{R,\max} = QT \frac{L}{L+\lambda}. \tag{A.4}$$

Empirically, the escape length L and the optical absorption length λ are nearly equal for CsI. If exactly so, then $Y_{R,\max} = QT/2$. Now $Y_{R,\max}$ is what is usually called the observed quantum efficiency, so we see that if values of Y are reported near 0.5 this implies the intrinsic quantum efficiency is essentially 100%.

For a semitransparent photocathode the yield Y_S is

$$Y_S = \frac{Q}{\lambda}\int_0^d dx\, G(x)\, e^{-(d-x)/\lambda}$$

$$= QT\frac{L}{L-\lambda}(e^{-d/L} - e^{-d/\lambda}). \qquad (A.5)$$

The maximum yield is attained with a cathode of thickness d_0 such that $e^{-d_0/\lambda} = (\lambda/L)\, e^{-d_0/L}$, and the maximum value is

$$Y_{S,max} = QTe^{-d_0/L}. \qquad (A.6)$$

In the approximation that $L \approx \lambda$ we have the optimal cathode thickness as $d_0 = L$, and $Y_{S,max} = QT/e$. In this same approximation that ratio of maximum yields from semitransparent and reflective photocathodes is

$$\frac{Y_{S\,max}}{Y_{R,max}} = \frac{2}{e} = 0.74 \qquad (L \approx \lambda). \qquad (A.7)$$

We close this section with the qualitative observation that since the yield of semitransparent cathodes depends on the difference between the escape length L and the optical absorption length λ while that of reflective cathodes depends on the sum, the former is much more sensitive to the details of electron transport.

A.2. A diffusion model

A tacit assumption of the exponential model was that the electron transport is the average effect of a large number of nearly elastic collisions. The resulting random walk should be well described as a diffusion process so long as the number of collisions is indeed very large.

The first form of diffusion model that we consider is one articulated by Chen et al. [26]. The one-dimensional density of electrons $\rho(x, t)$ is subject to lossless diffusion described by a diffusion coefficient D. That is, the flux of electrons across the surface x = const. is

$$j = -D\frac{\partial\rho}{\partial x}. \qquad (A.8)$$

Combining this with the equation of continuity,

$$\frac{\partial\rho}{\partial t} = -\frac{\partial\rho}{\partial x}, \qquad (A.9)$$

we arrive at the lossless diffusion equation

$$\frac{\partial\rho}{\partial t} = D\frac{\partial^2\rho}{\partial x^2}. \qquad (A.10)$$

Loss of electrons is simply modelled by a decay constant τ according to

$$\frac{\partial\rho}{\partial t} = -\frac{\rho}{\tau}. \qquad (A.11)$$

Combining Eqs. (A.10) and (A.11) we arrive at the lossy diffusion equation:

$$\frac{\partial\rho}{\partial t} = D\frac{\partial^2\rho}{\partial x^2} - \frac{\rho}{\tau}. \qquad (A.12)$$

For boundary conditions we suppose that the surfaces at $x = 0$ and $x = d$ of the photocathode are perfect sinks (transmission coefficient $T = 1$), so that

$$\rho(0, t) = 0 = \rho(d, t). \qquad (A.13)$$

For the initial condition that a single electron is created at x_0 at $t = 0$ we have

$$\rho(x_0, 0) = \delta(x_0). \qquad (A.14)$$

The diffusion equation (A.12) then has the solution

$$\rho(x, t) = \frac{2}{d}e^{-t/\tau}\sum_n \sin\frac{n\pi x_0}{d} \times \sin\frac{n\pi x}{d}e^{-Dn^2\pi^2 t/d^2}. \qquad (A.15)$$

However, we are really interested in the flow of electrons across the surface $x = 0$ due to the electron initially at x, which is just the time integral of the flux:

$$G(x) = \int_0^\infty dt\, j(0, t)$$

$$= -\frac{2}{d}\sum_n \frac{n\pi/d}{(n\pi/d)^2 + 1/L^2}\sin\frac{n\pi x}{d}, \qquad (A.16)$$

where $L \equiv \sqrt{D\tau}$ emerges as the characteristic escape length. It is "well known" that this series can be summed to give

$$G(x) = \frac{\sinh((d-x)/L)}{\sinh(d/L)}. \qquad (A.17)$$

For thick films the escape probability becomes

$$G(x) \approx e^{-x/L} \qquad (d - x \gg L), \qquad (A.18)$$

just as for the exponential model (Eq. (A.1)). However, for thin films,

$$G(x) \approx 1 - x/d \qquad (d \ll L). \qquad (A.19)$$

That is, an electron produced at the surface of a thin film is supposed to have 100% probability of escaping, even if it is initially heading into the film. But if the film is thinner than some characteristic scattering length it is doubtful that the electron will reverse direction before arriving at the other surface of the film. This appears to be the main defect of the diffusion model.

The yield of electrons from a reflective photocathode is calculated as in the previous section, but using Eq. (A.17) for $G(x)$, to be

$$Y_R = \frac{QL}{2\sinh(d/L)} \times \left(\frac{e^{d/L} - e^{-d/\lambda}}{L+\lambda} - \frac{e^{-d/L} - e^{-d/\lambda}}{L-\lambda}\right). \qquad (A.20)$$

For thick films the maximum yield is

$$Y_{R,\max} = \frac{QL}{L+\lambda}, \tag{A.21}$$

exactly as found in Eq. (A.4) for the exponential model.

Likewise the yield of electrons from a semitransparent photocathode is found to be

$$Y_S = \frac{QL}{2\sinh(d/L)} \times \left(\frac{1-e^{d/L-d/\lambda}}{L-\lambda} - \frac{1-e^{-d/L-d/\lambda}}{L+\lambda} \right). \tag{A.22}$$

For the case that $L \approx \lambda$ the maximum yield is attained for $d \approx 1.23L$, at which $Y_{S,\max} \approx 0.25Q$. This yield is low because the diffusion model claims there is no chance for collecting at $x = 0$ an electron produced at $x = d$ where the photon absorption is largest.

This result seems too severe. Indeed, a Monte Carlo calculation of the Boltzmann transport equation for CsI films [27] indicates that the probability of collecting electrons that originate near the opposite surface is 0.1–0.4. Hence we consider another version of the diffusion model in the next section.

A.3. The diffusion model of Kane

A generalization of the diffusion model has been given by Kane [28]; see also ref. [29].

In this model we include a scattering length

λ_{ep} for electron–phonon interactions, (A.23)

and another scattering length

λ_{ee} for electron–electron interactions. (A.24)

An important assumption of the model is that if an electron suffers a collision with another electron it loses so much energy that it can no longer escape. On the other hand, the electron–phonon collisions are taken to be elastic.

Then an electron produced at depth x has probability

$$P_0(x) = (T/2)\, e^{-x/\lambda_e} \tag{A.25}$$

of reaching the surface with zero scatters along the way and then escaping. In this, λ_e is the combined scattering length

$$\frac{1}{\lambda_e} = \frac{1}{\lambda_{ep}} + \frac{1}{\lambda_{ee}}. \tag{A.26}$$

As before, T is the surface-transmission coefficient. The factor $1/2$ in Eq. (A.25) occurs because an electron can reach the surface with zero scatters only if it is heading towards the surface initially.

The total probability $G(x)$ that an electron produced at x escapes from the surface at $x = 0$ is taken at the sum over the probabilities that it escapes with exactly n electron–phonon scatters along the way:

$$G(x) = \sum_n P_n(x). \tag{A.27}$$

(To escape, an electron must always have zero electron–electron scatters.) Each probability $P_n(x)$ can be obtained from $P_{n-1}(x)$ by the integral equation

$$P_n(x) = \int_0^x P_{n-1}(y)\, e^{-(x-y)/\lambda_e} \frac{dy}{2\lambda_{ep}} + \int_x^d P_{n-1}(y)\, e^{-(y-x)/\lambda_e} \frac{dy}{2\lambda_{ep}}. \tag{A.28}$$

In this the electron is produced at x and drifts to y where it suffers its first electron–phonon collision in the interval dy. It then reaches the surface after $n-1$ additional electron–phonon collisions with probability $P_{n-1}(y)$. The two terms arise according to the initial direction of the electron.

Kane [28] notes that in principle there should be additional terms in Eq. (A.28) corresponding to the cases that the electron reaches a surface and bounces off before suffering its first electron–phonon collision. We ignore these terms, which are important only for extremely thin films.

By summing Eq. (A.28) from $n = 1$ to ∞ and adding $P_0(x)$ we obtain an integral equation for $G(x)$:

$$G(x) = \frac{1}{2\lambda_{ep}} \left(\int_0^x G(y)\, e^{-(x-y)/\lambda_e}\, dy + \int_x^d G(y)\, e^{-(y-x)/\lambda_e}\, dy \right) + P_0(x). \tag{A.29}$$

Kane cleverly noted that on differentiating this equation twice we obtain the differential equation

$$G'' = G/L^2, \tag{A.30}$$

where we introduce the escape length L as

$$\frac{1}{L^2} = \frac{1}{\lambda_e^2} - \frac{1}{\lambda_e \lambda_{ep}} = \frac{1}{\lambda_{ep}\lambda_{ee}} + \frac{1}{\lambda_{ee}^2}. \tag{A.31}$$

Clearly Eq. (A.30) has the solution

$$G(x) = A\, e^{x/L} + B\, e^{-x/L}. \tag{A.32}$$

Coefficients A and B can be determined by substituting this solution into Eq. (A.29) at the boundaries $x = 0$ and d. Thus

$$G(0) = A + B = \frac{1}{2\lambda_{ep}} \int_0^d (A\, e^{x/L} + B\, e^{-x/L})\, e^{-x/\lambda_e}\, dx + \frac{T}{2} \tag{A.33}$$

$$= \frac{L\lambda_e}{2\lambda_{ep}} \left(A \frac{1-e^{d/L-d/\lambda_e}}{L-\lambda_e} + B \frac{1-e^{-d/L-d/\lambda_e}}{L+\lambda_e} \right) + \frac{T}{2},$$

and

$$G(d) = A\,\mathrm{e}^{d/L} + B\,\mathrm{e}^{-d/L}$$
$$= \frac{1}{2\lambda_{ep}}\int_0^d (A\,\mathrm{e}^{x/L} + B\,\mathrm{e}^{-x/L})\,\mathrm{e}^{-(d-x)/\lambda_e}\,\mathrm{d}x + \frac{T}{2}\mathrm{e}^{-d/\lambda_e} \tag{A.34}$$
$$= \frac{L\lambda_e}{2\lambda_{ep}}\left(A\frac{\mathrm{e}^{d/L} - \mathrm{e}^{-d/\lambda_e}}{L+\lambda_e} + B\frac{\mathrm{e}^{-d/L} - \mathrm{e}^{-d/\lambda_e}}{L-\lambda_e}\right) + \frac{T}{2}\mathrm{e}^{-d/\lambda_e}.$$

This leads to lengthy expressions for A and B in general. (We do not find the forms reported in Eqs. (A9-10) of ref. [29].)

To obtain relatively simple forms for A and B we restrict ourselves to materials, such as CsI, for which

$$\lambda_{ep} \ll \lambda_{ee} \qquad \text{(insulators)}. \tag{A.35}$$

We introduce the small parameter C defined by

$$C^2 \equiv \lambda_{ep}/\lambda_{ee}, \tag{A.36}$$

and will keep terms in A and B only to order C. In this approximation

$$L = \lambda_{ep}/C \qquad \text{and} \qquad \lambda_e = \lambda_{ep}. \tag{A.37}$$

We also suppose that $d \gg \lambda_e$, i.e., the cathode thickness is much greater than an electron scattering length, so we may ignore all terms in $\mathrm{e}^{-d/\lambda_e}$. Then Eqs. (A.33) and (A.35) become

$$A(1-C) + B(1+C) = T, \tag{A.38}$$

and

$$A\,\mathrm{e}^{d/L}(1+C) + B\,\mathrm{e}^{-d/L}(1-C) = 0. \tag{A.39}$$

We now find that

$$G(x) = T\frac{\sinh\dfrac{d-x}{L} + C\,\mathrm{e}^{(d-x)/L}}{\sinh\dfrac{d}{L} + C\left(\mathrm{e}^{d/L} + \cosh\dfrac{d}{L}\right)}. \tag{A.40}$$

We see that as parameter C goes to zero we recover the previous diffusion model. For thick cathodes the escape probability goes to

$$G(x) = T\,\mathrm{e}^{-x/L}(1-C) \qquad (d \gg L), \tag{A.41}$$

and for thin cathodes

$$G(x) = T\frac{(d-x)/L + C}{d/L + 2C}, \qquad (d \ll L). \tag{A.42}$$

In this model, if d/L becomes less than C we note that $G(x) \to T/2$. Since $\lambda_e \approx CL$, this limit corresponds to $d < \lambda_e$ and so the electrons reach the surface without scattering, which implies the escape probability should be just $T/2$. Hence the diffusion model of Kane has better behavior for very thin cathodes that does the first diffusion model.

We complete our discussion of this model by calculating the yields for reflective and semitransparent cathodes:

$$Y_R = \frac{QL}{2\left[\sinh(d/L) + C\left(\mathrm{e}^{d/L} + \cosh(d/L)\right)\right]} \times\left((1+2C)\frac{\mathrm{e}^{d/L} - \mathrm{e}^{-d/\lambda}}{L+\lambda} - \frac{\mathrm{e}^{-d/L} - \mathrm{e}^{-d/\lambda}}{L-\lambda}\right), \tag{A.43}$$

and

$$Y_S = \frac{QL}{2\left[\sinh(d/L) + C\left(\mathrm{e}^{d/L} + \cosh(d/L)\right)\right]} \times\left((1+2C)\frac{1 - \mathrm{e}^{d/L - d/\lambda}}{L-\lambda} - \frac{1 - \mathrm{e}^{-d/L - d/\lambda}}{L+\lambda}\right). \tag{A.44}$$

References

[1] J. Séguinot and T. Ypsilantis, Nucl. Instr. and Meth. 142 (1977) 377.
[2] V. Peskov et al., Nucl. Instr. and Meth. A 269 (1988) 149.
[3] V. Dangendorf et al., Nucl. Instr. and Meth. A 289 (1990) 322.
[4] J Séguinot et al., Nucl. Instr. and Meth. A 297 (1990) 133.
[5] B. Hoeneisen, D.F. Anderson and S. Kwan, Nucl. Instr. and Meth. A 302 (1991) 447.
[6] G. Charpak et al., Nucl. Instr. and Meth. A 307 (1991) 63.
[7] V. Dangendorf et al., Nucl. Instr. and Meth. A 308 (1991) 519.
[8] G. Charpak et al., Nucl. Instr. and Meth. A 310 (1991) 128.
[9] S. Kwan and D.F. Anderson, Nucl. Instr. and Meth. A 309 (1991) 190.
[10] Y. Giomataris et al., Nucl. Instr. and Meth. A 323 (1992) 431.
[11] G. Charpak, V. Peskov and F. Sauli, Nucl. Instr. and Meth. A 323 (1992) 445.
[12] H. Ehrlichmann, E. Michel and P. Križan, Nucl. Instr. and Meth. A 323 (1992) 452.
[13] M. Starič et al., Nucl. Instr. and Meth. A 323 (1992) 457.
[14] D.F. Anderson et al., Nucl. Instr. and Meth. A 323 (1992) 626.
[15] A. Akkerman et al., J. Appl. Phys. 72 (1992) 5429.
[16] N.S. Lockyer et al., Nucl. Instr. and Meth. A 332 (1993) 142.
[17] C. Lu, K.T. McDonald and Y. Zhu, Nucl. Instr. and Meth. A 334 (1993) 328.
[18] R.A. Holroyd et al., Measurement of the Absorption Length and Absolute Quantum Efficiency of TMAE and

TEA from Threshold to 120 nm, Nucl. Instr. and Meth. A 261 (1987) 440.
[19] G.W. Goetze, Transmission Secondary Emission from Low Density Deposites of Insulators, Adv. Elec. Elec. Phys. 16 (1962) 145.
[20] G.W. Goetze et al., Field-Enhanced Secondary Electron Emission from Film of Low Density, J. Appl. Phys. 35 (1964) 482.
[21] G.W. Goetze, Secondary Electron Conduction (SEC) and Its Application to Photo-electronic Image Devices, Adv. Elec. Elec. Phys. 22A (1966) 219.
[22] D.F. Anderson, A Photoionization Detector for the Detection of Xenon Light, IEEE Trans. Nucl. Sci. 28 (1981) 842.
[23] H. Bräuning et al., Investigation of CsI and CsI-TMAE VUV-Photocathodes in Vacuum and Gas, WIS-92/62/Aug-PH, submitted to Nucl. Instr. and Meth.
[24] R. Arnold et al., Nucl. Instr. and Meth. A 270 (1988) 289.
[25] F.M. Smith, Measurement of sheet resistivities with the four-point probe, Bell System Technical Journal (May 1958).
[26] D.M. Chen et al., Phys. Rev. B 31 (1985) 4123.
[27] J. Llacer and E.L. Garwin, J. Appl. Phys. 40 (1969) 2766.
[28] E.O. Kane, Phys. Rev. 147 (1966) 335.
[29] B.L. Henke, J.P. Knauer and K. Premaratne, J. Appl Phys. 52 (1981) 1509.